Results of an all-sky high-frequency Einstein@Home search for continuous gravitational waves in LIGO 5th Science Run

Avneet Singh[1,2,3,a], Maria Alessandra Papa[1,2,4,b], Heinz-Bernd Eggenstein[2,3], Sylvia Zhu[1,2], Holger Pletsch[2,3], Bruce Allen[2,4,3], Oliver Bock[2,3], Bernd Maschenchalk[2,3], Reinhard Prix[2,3], Xavier Siemens[4]

[1] *Max-Planck-Institut für Gravitationsphysik, am Mühlenberg 1, 14476, Potsdam-Golm*
[2] *Max-Planck-Institut für Gravitationsphysik, Callinstraβe 38, 30167, Hannover*
[3] *Leibniz Universität Hannover, Welfengarten 1, 30167, Hannover*
[4] *University of Wisconsin-Milwaukee, Milwaukee, Wisconsin 53201, USA*

(Dated: August 31, 2016)

We present results of a high-frequency all-sky search for continuous gravitational waves from isolated compact objects in LIGO's 5th Science Run (S5) data, using the computing power of the Einstein@Home volunteer computing project. This is the only dedicated continuous gravitational wave search that probes this high frequency range on S5 data. We find no significant candidate signal, so we set 90%-confidence level upper-limits on continuous gravitational wave strain amplitudes. At the lower end of the search frequency range, around 1250 Hz, the most constraining upper-limit is 5.0×10^{-24}, while at the higher end, around 1500 Hz, it is 6.2×10^{-24}. Based on these upper-limits, and assuming a fiducial value of the principal moment of inertia of 10^{38}kg m^2, we can exclude objects with ellipticities higher than roughly 2.8×10^{-7} within 100 pc of Earth with rotation periods between 1.3 and 1.6 milliseconds.

I. INTRODUCTION

Ground-based gravitational wave (GW) detectors will be able to detect a continuous gravitational wave signal from a spinning deformed compact object provided that it is spinning with a rotational period between roughly 1 and 100 milliseconds, that it is sufficiently close to Earth and sufficiently "bumpy". Blind searches for continuous gravitational waves probe the whole sky and broad frequency ranges, looking for this type of objects.

In this paper, we present the results of an all-sky Einstein@Home search for continuous, nearly monochromatic, high-frequency gravitational waves in data from LIGO's 5th Science Run (S5). A number of searches have been carried out on LIGO data [2, 4, 5, 7–9] targeting lower frequency ranges. The only other search covering frequencies up to 1500 Hz was conducted on S6 data [10] taken at least 3 years apart from the data used here. Our search results are only 33% less sensitive than those of Abbot *et al* [10], even though the S5 data is less sensitive than the S6 data by more than a factor of 2. The search method presented here anticipates the procedure that will be used on the advanced detector (aLIGO) data.

This search can be considered an extension of the S5 Einstein@Home search [2] although it employs a different search technique: this search uses the *Global Correlation Transform* (GCT) method to combine results from coherent $\mathcal{F}$*-statistic* searches [15, 16], as opposed to the previous Einstein@Home search [2] that employed the *Hough-transform* method to perform this combination. In the end, at fixed computing resources, these two search methods are comparable in sensitivity. However, a semi-coherent $\mathcal{F}$*-statistic* search is more efficient when considering a broad spin-down range, and for the Einstein@Home searches we have decided to adopt it as our "work horse".

We do not find any significant signal(s) among the set of searched waveforms. Thus, we set 90%-confidence upper-limits on continuous gravitational wave strain amplitudes; near the lower end of the search frequency range between 1253.217–1255.217 Hz, the most constraining upper-limit is 5.0×10^{-24}, while toward the higher end of the search frequency range nearing 1500 Hz, the upper-limit value is roughly 6.2×10^{-24}. Based on these upper-limits, we can exclude certain combinations of signal frequency, star deformation (ellipticity) and distance values. We show with this search that even with S5 data from the first generation of GW detectors, such constraints do probe interesting regions of source parameter space.

II. THE DATA

The LIGO gravitational wave network consists of two detectors, H1 in Hanford (Washington) and L1 in Livingston (Louisiana), separated by a 3000-km baseline. The S5 run lasted roughly two years between GPS time 815155213 sec (Fri, Nov 04, 16:00:00 UTC 2005) and 875145614 sec (Sun, Sep 30, 00:00:00 UTC 2007). This search uses data spanning this observation period, and during this time, H1 and L1 had duty-factors of 78% and

[a]email: avneet.singh@aei.mpg.de
[b]email: maria.alessandra.papa@aei.mpg.de

66% respectively [3, 6]. The gaps in this data-set are due to environmental or instrumental disturbances, or scheduled maintenance periods.

We follow [2, 4], where the calibrated and high-pass filtered data from each detector is partitioned in 30-minute chunks and each chunk is Fourier-transformed after the application of a steep Tukey window. The set of **S**hort (time-baseline) **F**ourier **T**ransforms (SFT) that ensues, is the input data for our search.

We further follow [2], where frequency bands known to contain spectral disturbances have been removed from the analysis. In fact, such data has been substituted with fake Gaussian noise at the same level as the neighboring undisturbed data; in Table III, we list these bands.

III. THE SEARCH

The search presented here is similar to the search on S6 data, reported in [9]. Our reference target signal is given by (1)-(4) in [7]; at emission, the signal is nearly monochromatic, typically with a small spin-down. The signal waveform in the detector data is modulated in frequency because of the relative motion between the compact object and the detector; a modulation in amplitude also occurs because of the variation of the sensitivity of the detector with time across the sky.

The most sensitive search technique that one could use is a fully-coherent combination of the detectors' data, matched to the waveform that one is looking for. The (amplitude) sensitivity of such a method increases with the square-root of the time-span of the data used. However, the computational cost to resolve different waveforms increases very rapidly with increasing time-span of the data, and this makes a fully-coherent search over a large frequency range computationally unfeasible when using months of data. This is the main reason why semi-coherent search methods have been developed. These methods perform coherent searches over shorter stretches of data, called segments, and then combine the results with incoherent techniques.

This search covers waveforms from the entire sky, with frequencies in a 250 Hz range from 1249.717 Hz to 1499.717 Hz, and with a first-order spin-down between -2.93×10^{-9} Hz/s and 5.53×10^{-10} Hz/s, similar to previous Einstein@Home searches. We use a stack–slide semi-coherent search procedure implemented with the GCT method [15, 16]. The data is divided into $N_{\rm seg}$ segments, each spanning $\mathrm{T_{coh}}$ in time. The coherent multi-detector $\mathcal{F}$-statistic [11] is computed on each segment for all the points on a coarse $\lambda_{\rm c} \equiv (f_{\rm c}, \dot{f}_{\rm c}, \alpha_{\rm c}, \delta_{\rm c})$ signal waveform parameter grid, and then results from the individual segments are summed, one per segment, to yield the final core detection-statistic $\overline{\mathcal{F}}$, as shown in (1); α, δ are the equatorial sky coordinates of the source position, while f and $\dot{f}$ are the frequency and first-order spin-down of the signal respectively. Depending on which $\lambda_{\rm c}$ parameter points are taken on the coarse grid for each segment in this sum, the result will approximate the detection-statistic computed on a λ_f parameter point on a finer grid:

$$\overline{\mathcal{F}}(\lambda_f) := \frac{1}{N_{\rm seg}} \sum_{i=1}^{N_{\rm seg}} \mathcal{F}(\lambda_{\rm c}^i) \tag{1}$$

In a stack–slide search in Gaussian noise, $N_{\rm seg} \times 2\overline{\mathcal{F}}$ follows a $\chi^2_{4N_{\rm seg}}$ chi-squared distribution with $4N_{\rm seg}$ degrees of freedom.

The most important search parameters are then: $N_{\rm seg}$, $\mathrm{T_{coh}}$, the signal parameter search grids $\lambda_{\rm c}$, λ_f, the total spanned observation time $\mathrm{T_{obs}}$, and finally the ranking statistic used to rank parameter space cells i.e. $2\overline{\mathcal{F}}$.

The grid-spacing in frequency δf and spin-down $\delta \dot{f}$ are constant over the search range. The same frequency spacing and sky grid is used for the coherent analysis and in the incoherent summing. The spin-down spacing of the incoherent analysis is finer by a factor of γ with respect to that of the coherent analysis. In Table I, we summarize the search parameters.

The sky-grid for the search is constructed by tiling the projected equatorial plane uniformly with squares of edge length $d_{\rm sky}$. The length of the edge of the squares is a function of the frequency f of the signal, and parameterized in terms of a so-called sky-mismatch parameter ($\mathrm{m_{sky}}$) as

$$d_{\rm sky} = \frac{1}{f} \frac{\sqrt{\mathrm{m_{sky}}}}{\pi \tau_{\rm E}} \tag{2}$$

where $\tau_{\rm E} = 0.021$ seconds and $\mathrm{m_{sky}} = 0.3$, also given in Table I. The sky-grids are constant over 10 Hz-wide frequency bands, and are calculated for the highest frequency in the band. In Fig.1, we illustrate an example of the sky-grid. The total number of templates in 50 mHz bands as a function of frequency is shown in Fig.2. This search explores a total of 5.6×10^{16} waveform templates across the $\lambda_f \equiv (f_f, \dot{f}_f, \alpha_f, \delta_f)$ parameter space.

The search is divided into work-units (WU), each searching a very small sub-set of template waveforms. The WU are sent to Einstein@Home volunteers and each WU occupies the volunteer/host computer for roughly 6 hours. One such WU covers a 50 mHz band, the entire spin-down range, and 139–140 points in the sky. 6.4 million different WU are necessary to cover the whole parameter space. Each WU returns a ranked list of the most significant 10^4 candidates found in the parameter space that it searched.

IV. IDENTIFICATION OF UNDISTURBED BANDS

In Table III, we list the central frequencies and bandwidths of SFT data known to contain spectral lines from instrumental artefacts. These frequency regions

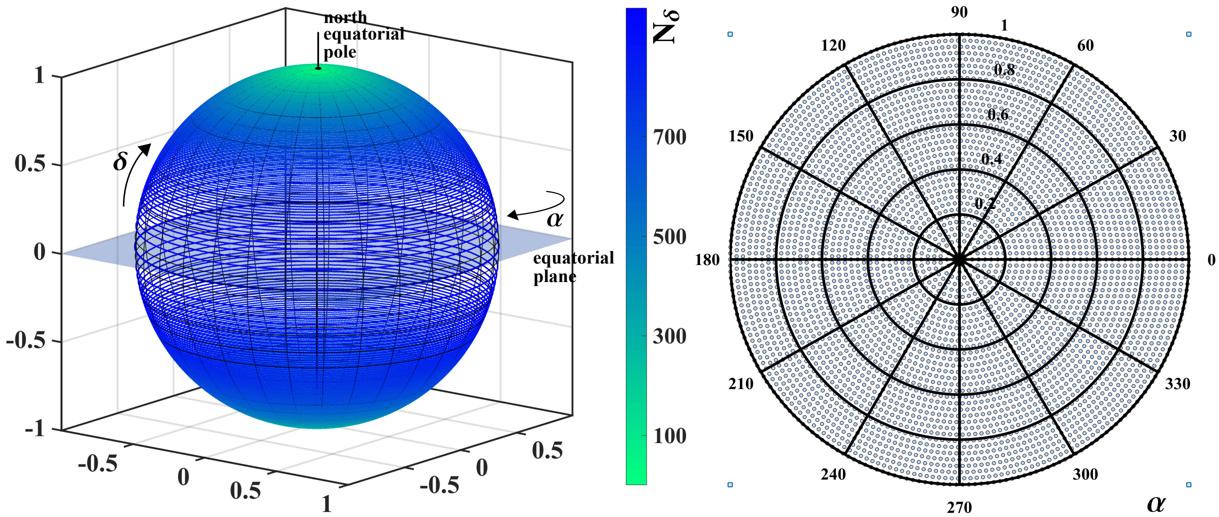

FIG. 1. Tilling of sky-grid for the frequency band 1240-1250 Hz; $d_{\text{sky}} = 6.6 \times 10^{-4}$ for this band. In the left panel, we show the sky-grid points on the celestial sphere; the color-code traces the number of sky-grid points, N_δ, as a function of equatorial latitude δ. The right panel is a polar plot of the northern equatorial hemisphere of the same sky-grid but with density scaled down by a factor of 4 to allow for better viewing. In the polar plot, $\theta = \alpha$ and $r = \cos(\delta)$.

were identified before the Einstein@Home run, and we were able to replace the corresponding data with Gaus-
Consequently, some search results have contributions from this 'fake data'. The intervals in signal-frequency where the search results come entirely from fake data are indicated as *All Fake Data* in Table IV. In these intervals of signal-frequency, we effectively do not have search results. The other three columns in Table IV provide signal-frequency intervals where results *might* have contributions from fake data. In these regions, depending on the signal parameters, the detection efficiency might be affected.

Quantity	**Value**
T_{coh} (hours)	30.0
T_{obs} (days)	653.18
t_{ref} (GPS seconds)	847063082.5
N_{seg}	205
δf_{c} (Hz)	6.71×10^{-6}
$\delta \dot{f}_{\text{c}}$ (Hz/s)	5.78×10^{-10}
γ	1399
m_{sky}	0.30

TABLE I. Search parameters for the search. t_{ref} is the reference time that defines the frequency and spin-down values.

Despite the removal of known disturbances from the data, it still contains unknown noise artefacts producing $2\overline{\mathcal{F}}$ values that do not follow the expected distribution for Gaussian noise. These artefacts usually have narrow-band characteristics; we identify such "disturbed" signal-frequency intervals in the search results and exclude them

sian noise matching the noise level of neighbouring quiet bands.

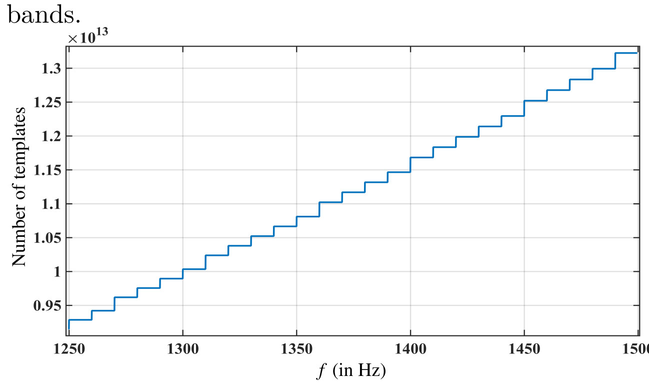

FIG. 2. Number of templates searched in 50 mHz bands. The variation in template count arises from the variation is number of sky-grid points every 10 Hz in frequency. Each 50 mHz band contributes roughly 6.3×10^7 templates in frequency and spin-down (on the finer grid refined by refinement factor γ.)

from further consideration. The benefit of such exclusions is that, in the remaining "undisturbed" bands, we can rely on semi-analytic predictions for the significance of the observed $2\overline{\mathcal{F}}$ values, and we can set a uniform detection criterion across the entire parameter space. It is true that we forego the possibility of detecting a signal in the disturbed frequency intervals. However, in order to perform reliable analyses in these intervals, ad-hoc studies and tuning of the procedures would need to be performed on each disturbed band separately and these would be very time-consuming. Since the undisturbed intervals in data comprise over 95% of the total data, we believe that ignoring the disturbed bands for this search is a reasonable choice. In the future, a focused effort on the analysis of the disturbed bands could attempt to recover some sensitivity in those regions.

The identification of undisturbed bands is carried out via a *visual inspection method*. This visual inspection of the data is performed by two scientists who look at various distributions of the $2\overline{\mathcal{F}}$ values in the $(f, \dot{f})$ parameter space in 50 mHz bands. They rank these 50 mHz bands with 4 numbers: 0,1,2,3; a '0' ranking marks the band as "undisturbed", a '3' ranks the band as "disturbed", and rankings of '1' or '2' mark the band as "marginally disturbed". A 50 mHz band is eventually considered to be undisturbed if it is marked as '0' by both scientists. The criteria used for this inspection are based on training-sets of real data containing simulated signals. These criteria are designed to exclude disturbed set of results while retaining data sets with signal-like properties, and to err on the side of being conservative in terms of not falsely dismissing signals. A significant part of this visual inspection work can be automated [20], but at the time of this search, the procedure had not been fully tested and tuned. In Fig.3, we empirically illustrate these criteria using three examples. Following this procedure, 3% of the total 5000 50 mHz bands are marked as "disturbed" by visual inspection. These excluded bands are listed in Table V (Type D), together with the 50 mHz bands excluded as a result of the cleaning of known disturbances above (Type C), i.e. marked as "All Fake Data" in Table IV. In consequence to these exclusions, there exist 0.5 Hz bands comprising results from less than ten 50 mHz bands. We define 'fill-level' as the percentage of 50 mHz bands that contribute to the results in 0.5 Hz intervals, where 100% fill-level signifies contribution by all ten 50 mHz bands. In Fig.7, we show the distribution of fill-levels for the 0.5 Hz bands searched.

In Fig.4, we plot the loudest observed candidate i.e. the candidate with the highest $2\overline{\mathcal{F}}$ value in each 0.5 Hz band of the search frequency range. The loudest candidate in our search has a detection-statistic value of $2\overline{\mathcal{F}} = 5.846$ at a frequency of roughly 1391.667 Hz. In order to determine the significance of this loudest candidate, we compare it to the expected value for the highest detection-statistic in our search. In order to determine this expected value, we have to estimate the number of independent trials performed in the search i.e. total number of independent realizations of our detection-statistic $2\overline{\mathcal{F}}$.

The number of independent realizations of the detection-statistic, N_{trials}, in a search through a bank of signal templates is smaller than the total number of searched templates, $N_{\mathrm{templates}}$. We estimate N_{trials} as a function of frequency in 10 Hz frequency intervals. In each of these 10 Hz intervals, we fit the distribution of loudest candidates from 50 mHz bands to the expected distribution [1], and obtain the best-fitted value of N_{trials}. We perform this calculation in 10 Hz intervals since the sky-grids, along with $N_{\mathrm{templates}}$, are constant over 10 Hz frequency intervals. In Fig.5, we plot the ratio $\mathcal{R} = N_{\mathrm{trials}}/N_{\mathrm{templates}}$, as a function of frequency.

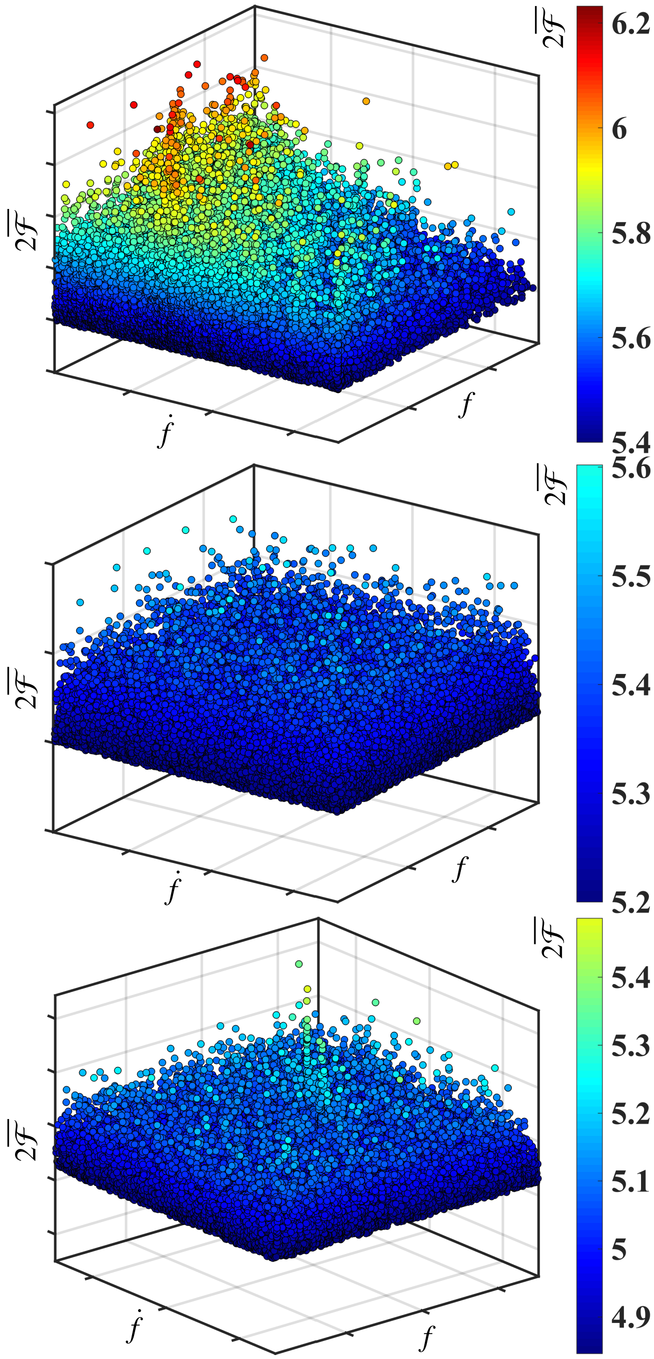

FIG. 3. We plot the color-coded $2\overline{\mathcal{F}}$ values on the z-axis in three 50 mHz bands. The top-most band is marked as "disturbed"; the middle band is an example of an "undisturbed" band; the bottom-most band is an example of an undisturbed band but containing a simulated continuous gravitational wave signal.

With $\mathcal{R}(f)$ in hand, we evaluate the expected value for the loudest detection-statistic ($2\overline{\mathcal{F}}_{\mathrm{exp}}$) in 0.5 Hz bands, and the standard deviation (σ_{exp}) of the associated distribution using (5)-(6) of [1], with $N_{\mathrm{seg}} = 205$ and $N_{\mathrm{trials}} = \mathcal{R}\, N_{\mathrm{templates}}$. Based on these values, we can

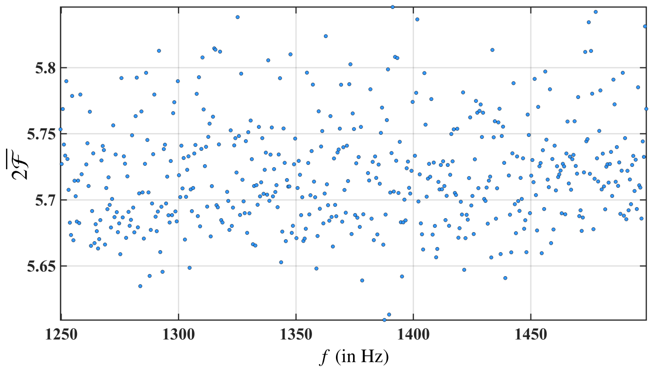

FIG. 4. Highest values of $2\overline{\mathcal{F}}$ in every 0.5 Hz band as a function of starting frequency of the band.

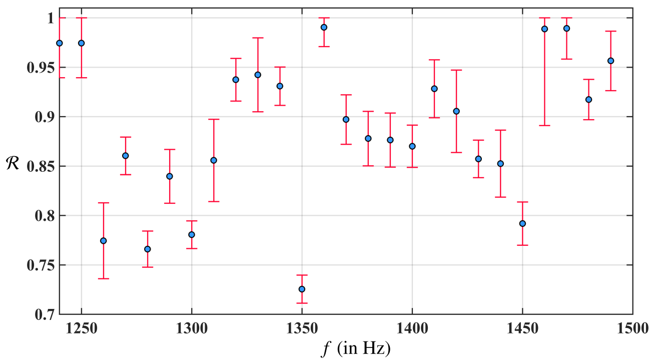

FIG. 5. Ratio $\mathcal{R} = N_{\rm trials}/N_{\rm templates}$ as a function of frequency in 10 Hz intervals. The error bars represent the 1-σ statistical errors from the fitting procedure described in the text.

estimate the significance of the observed loudest candidates (denoted by $2\overline{\mathcal{F}}_{\rm Loud}$) as the critical ratio (CR),

$$\mathrm{CR} := \frac{2\overline{\mathcal{F}}_{\rm Loud} - 2\overline{\mathcal{F}}_{\rm exp}}{\sigma_{\rm exp}}. \tag{3}$$

In Fig.6, we plot the CR values of the observed loudest candidates in 0.5 Hz bands as a function of frequency (top panel) and their distribution (bottom panel).

In this search, the overall loudest candidate with $2\overline{\mathcal{F}} = 5.846$ is also the most significant candidate, with $\mathrm{CR} = 3.05$. A deviation of 3.05σ from the expected $2\overline{\mathcal{F}}$ value would not be significant enough to claim a detection if we had only searched a single 0.5 Hz band. It is even less significant considering the fact that a total of 485 0.5 Hz bands were searched.

We define the p-value associated with a CR as the probability of observing that particular value of CR or higher by random chance in a search over one 0.5 Hz band, performed over $N_{\rm trials}$ independent trials using $N_{\rm seg}$ segments. In Fig.8, we see that the distribution of p-values associated with the loudest observed candidates in 0.5 Hz bands is consistent with what we expect from the noise-only scenario across the explored parameter space. In particular, we see in Fig.8 that across 485 0.5 Hz bands searched by our set up, we expect 2.3 ± 1.5 candidates at least as significant as $\mathrm{CR} = 3.05$ (p-value bin 10^{-2} for that band) by random chance, which makes our observed loudest candidate completely consistent with expectations from the noise-only case.

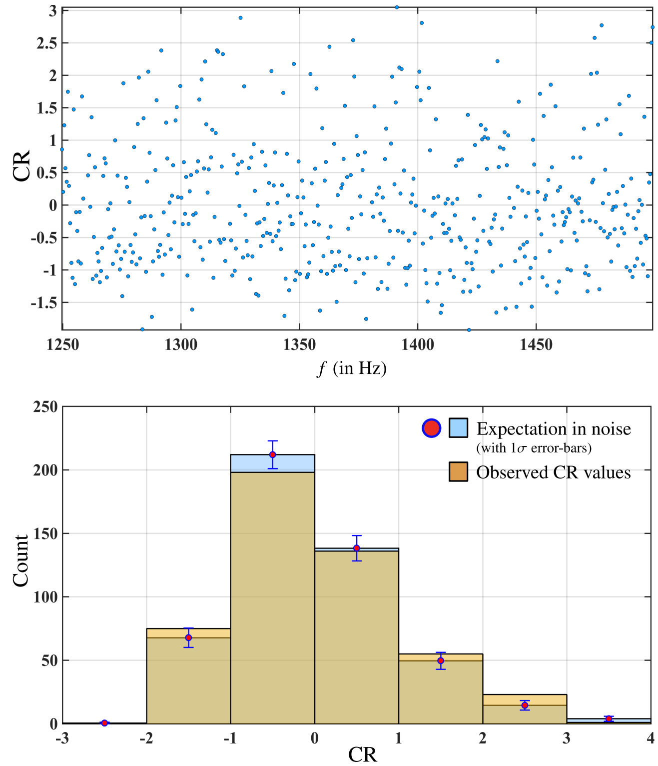

FIG. 6. In the top panel, we plot the significance of the loudest observed candidate in every 0.5 Hz band as a function of starting frequency of the band. In the bottom panel, we show the observed distribution of CR values (top brown histogram bars), and the expected distribution of CR values for pure noise for reference (bottom blue histogram bars with markers). The significance folds in the expected value for the loudest $2\overline{\mathcal{F}}$ and its standard deviation.

V. UPPER-LIMITS

Our search results do not deviate from the expectations from noise-only data. Hence, we set frequentist upper-limits on the maximum gravitational wave amplitude, $h_0^{90\%}$, from the target source population consistent with this null result at 90%-confidence in 0.5 Hz bands. Here, $h_0^{90\%}$ is the gravitational wave amplitude for which 90% of the target population of signals would have produced a value of the detection statistic higher than the observed value.

Ideally, in order to estimate the $h_0^{90\%}$ values in each 0.5 Hz band across the 250 Hz signal-frequency search range, we would perform Monte-Carlo injection-and-recovery simulations in each of those bands. However, this is computationally very intensive. Therefore, we per-

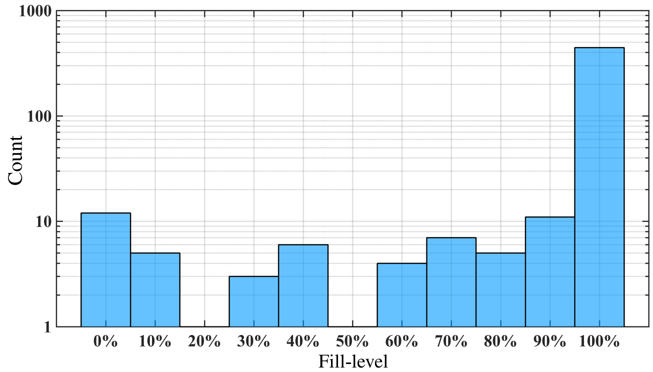

FIG. 7. Distribution of fill-levels of 0.5 Hz bands.

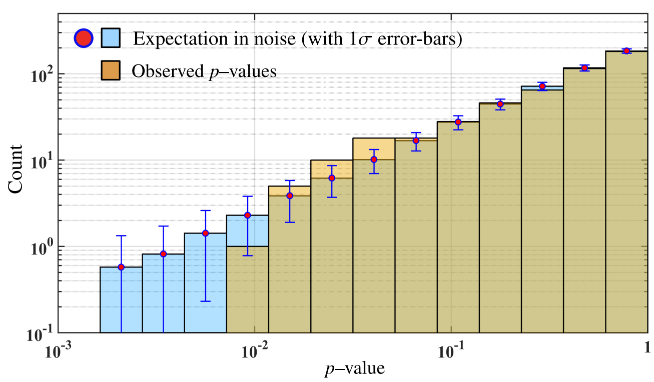

FIG. 8. p-values for the loudest observed candidates in 0.5 Hz bands in the data (top brown histogram bars), and the expected distribution of p-values for pure noise for reference (bottom blue histogram bars with markers).

form Monte-Carlo simulations in six 0.5 Hz bands spread evenly across the 250 Hz-wide frequency range, and in each of these six bands labeled by the index k, we estimate the $h_{0,\mathrm{CR}_i}^{90\%,k}$ upper-limit value corresponding to eight different CR_i significance bins for the putative observed loudest candidate: $(0.0, 0.5, 1.0, 1.5, 2.0, 2.5, 3.0, 3.5)$. In each of these six bands and for each of the eight detection criteria, we calculate the so-called 'sensitivity-depth', defined in [1]: $\mathcal{D}_{\mathrm{CR}_i}^{90\%,k}$. Lastly, we average these sensitivity-depths over the six bands and derive the average sensitivity-depth $\mathcal{D}_{\mathrm{CR}_i}^{90\%}$ for each detection criterion. The values of the sensitivity-depths range between $\mathcal{D}_{\mathrm{CR}_{0.0}}^{90\%} = 30.6\,\mathrm{Hz}^{-1/2}$ and $\mathcal{D}_{\mathrm{CR}_{3.5}}^{90\%} = 28.8\,\mathrm{Hz}^{-1/2}$. We use these $\mathcal{D}_{\mathrm{CR}_i}^{90\%}$ values to set upper-limits in the bands (labeled by j) where we have not performed any Monte-Carlo simulations as follows:

$$h_0^{90\%}(f_j) = \frac{\sqrt{S_h(f_j)}}{\mathcal{D}_{\mathrm{CR}_{i(j)}}^{90\%}} \qquad (4)$$

where, $\mathrm{CR}_i(j)$ is the significance bin i corresponding to the loudest observed candidate in the j-th frequency band, and $S_h(f_j)$ is the average amplitude spectral density of the data in that band, measured in $\mathrm{Hz}^{-1/2}$. The uncertainties on the $h_0^{90\%}$ upper-limit values introduced by this procedure amount to roughly 10% of the nominal $h_0^{90\%}$ upper-limit value. The final $h_0^{90\%}$ upper-limit values for this search, including an additional 10% calibration uncertainty, are given in Table II, and shown in Fig.9.

Note that we do not set upper limits in 0.5 Hz bands where the results are entirely produced with fake Gaussian data inserted by the cleaning procedure described in section IV; $h_0^{90\%}$ upper-limit values for such bands do not appear either in Table II, or in Fig.9. Moreover, there also exist 50 mHz bands that contain results contributed by entirely fake data as a result of the cleaning procedure, or that have been excluded from the analysis because they are marked as disturbed by the visual inspection method described in section IV. We mark the 0.5 Hz bands which host these particular 50 mHz bands with empty circles in Fig.9. In Table V, we provide a complete list of such 50 mHz bands, highlighting that the upper-limit values do not apply to these bands. Finally, we note that, because of the cleaning procedure, there exist signal-frequency bands where the search results *may* have contributions from some fake data. We list these signal-frequency ranges in Table IV. In line with the remarks in section IV, and for the sake of completeness, Table IV also contains the cleaned bands that featured under Type C in Table V, under the column header "All Fake Data".

VI. CONCLUSIONS

This search did not yield any evidence of continuous gravitational waves in the LIGO 5th Science Run data in the high-frequency range of 1250–1500 Hz. The lowest value for the upper-limit is 5.0×10^{-24} for signal frequencies between 1253.217–1255.217 Hz. We show in Fig.9 that these $h_0^{90\%}$ upper-limits are about 33% higher than the upper-limits[2] set [10] in the same frequency range but using S6 data. In this frequency range, the S6 run data is about a factor 2.4 more sensitive compared to the S5 data used in this search. We can express the $h_0^{90\%}$ upper-limits as bounds on the maximum distance from Earth within which we can exclude a rotating compact object emitting continuous gravitational waves at a given frequency f due to a fixed and non-axisymmetric mass quadrupole moment, characterised by ϵI, with I being the principal moment of inertia, and ϵ the ellipticity of the object. The GW-spindown is the fraction of spindown, $x|\dot{f}|$, responsible for continuous gravitational wave emission [14]. The ellipticity ϵ of the compact object nec-

[2] The upper-limit values of [10] have been re-scaled according to [19] in order to allow a direct comparison with our $h_0^{90\%}$ upper-limit results.

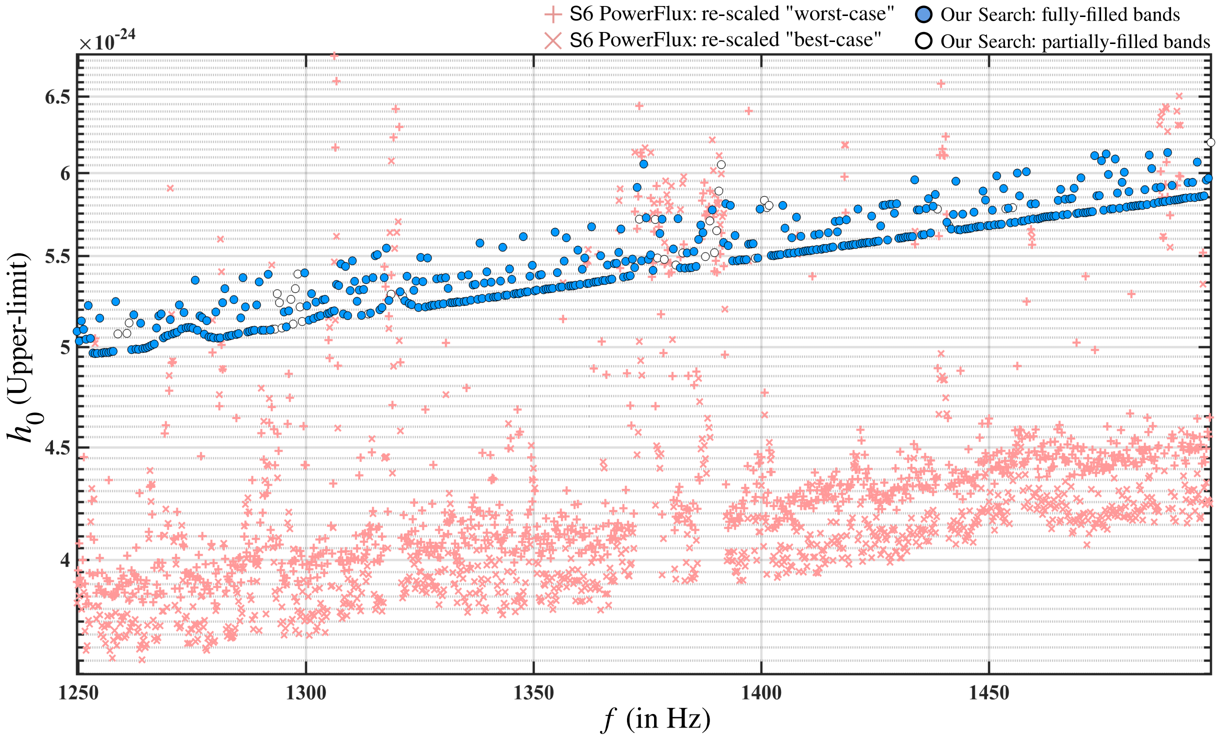

FIG. 9. 90%-confidence upper-limits on the gravitational wave amplitude for signals with frequency within 0.5 Hz bands, over the entire sky, and within the spin-down range of the search described in section III. The empty circular markers denote 0.5 Hz bands where the upper-limit value does not hold for all frequencies in that interval; the list of corresponding excluded frequencies is given in Table IV. For reference, we also plot the upper-limit results (with non-circular markers) from the only other high-frequency search [10], on significantly more sensitive S6 data. It should be noted that the upper-limits from the *PowerFlux* search [10] are set at 95%-confidence rather than 90%-confidence level as in this search, but refer to 0.25 Hz bands rather than 0.5 Hz bands.

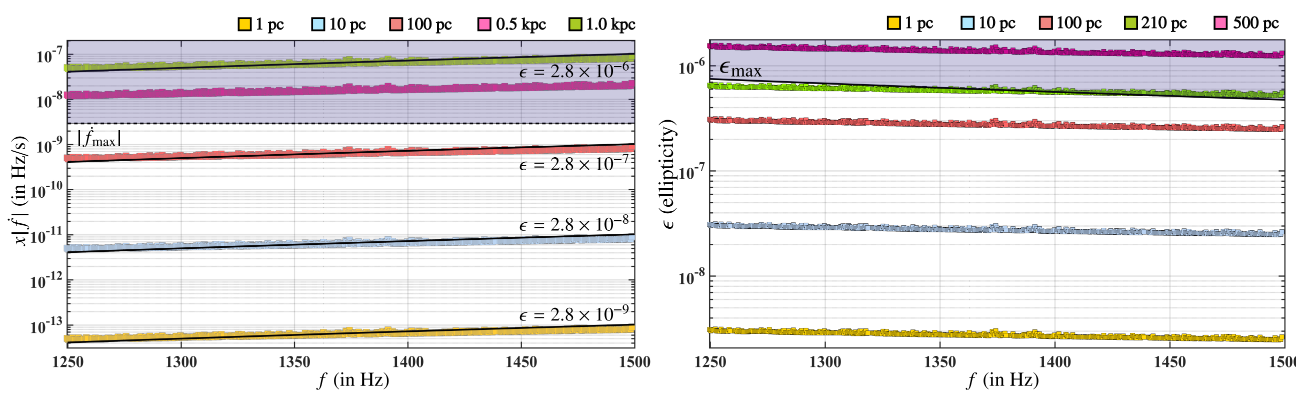

FIG. 10. Gravitational wave amplitude upper-limits recast as curves in the $(f, x|\dot{f}|)$-plane (left panel) for sources at given distances, where f is the signal-frequency and $x|\dot{f}|$ is the gravitational wave spin-down i.e. the fraction of the actual spin-down $|\dot{f}|$ that accounts for the rotational energy loss due to gravitational wave emission. We have superimposed the curves of constant ellipticity ϵ. The dotted line at $|\dot{f}_{\max}|$ indicates the maximum magnitude of searched spin-down, namely 2.93×10^{-9} Hz/s. The right panel shows the corresponding (f, ϵ) upper-limit curves for sources at various distances. The $\epsilon_{\max} = 41.3 \times f^{-5/2}$ curve is the ellipticity corresponding to the highest $|\dot{f}|$ searched.

essary to sustain such emission is given by

$$\epsilon(f, x|\dot{f}|) = \sqrt{\frac{5c^5}{32\pi^4 G}\frac{x|\dot{f}|}{I f^5}}, \qquad (5)$$

where c is the speed of light, G is the Gravitational constant. Moreover, since the gravitational wave amplitude for an object at a distance d, with an ellipticity ϵ given by (5), is expressed as

$$h_0(f, x|\dot{f}|, d) = \frac{1}{d}\sqrt{\frac{5IG}{2c^3}\frac{x|\dot{f}|}{f}}, \quad (6)$$

we can recast the $h_0^{90\%}$ upper-limit curves as $(f, x|\dot{f}|)$ curves, or as (f, ϵ) curves, both parametrised by different values of the distance d, as shown in Fig.V. We find that within 100 pc of Earth, our upper-limits exclude objects with ellipticities higher than roughly $2.8 \times 10^{-7}\left[\frac{10^{38}\mathrm{kg\,m}^2}{I}\right]$, corresponding to GW-spindown values between roughly 4.0×10^{-10} and 1.0×10^{-9} Hz/s. This value is well below the maximum elastic deformation that a relativistic star could sustain, see [12] and references therein.

The search presented here is probably the last all-sky search on S5 data, and by inspecting the higher frequency range for continuous gravitational wave emission, it concludes the Einstein@Home observing campaign on this data. Consistent with the recent results on S6 data [10], we also find no continuous GW signal in the S5 data. However, mechanisms for transient or intermittent GW emission have been proposed [13, 17, 18] which would not *a priori* exclude a signal that is "ON" during the S5 run and "OFF" during the S6 run. The estimates for the time-scales, frequencies and spin-downs of continuous gravitational wave signals from isolated neutron stars lasting weeks to months span a very broad range of values – orders of magnitude. There are several different mechanisms that could sustain such emission at a level that this search could have detected, and with spin-down values consistent with the total energy emitted in the process, and with the spin-down range spanned by this search.

VII. ACKNOWLEDGMENTS

Maria Alessandra Papa, Bruce Allen and Xavier Siemens gratefully acknowledge the support from NSF PHY Grant 1104902. All the post-processing computational work for this search was carried out on the ATLAS super-computing cluster at the Max-Planck-Institut für Gravitationsphysik/ Leibniz Universität Hannover. We also acknowledge the Continuous Wave Group of the LIGO Scientific Collaboration for useful discussions, and in particular, its chair Keith Riles for his careful reading of the manuscript. This paper has been assigned the LIGO Document Number P1600196.

* * *

Appendix A: Tabular data

1. Upper-limit $h_0^{90\%}$ values

f (in Hz)	$h_0^{90\%} \times 10^{24}$	f (in Hz)	$h_0^{90\%} \times 10^{24}$	f (in Hz)	$h_0^{90\%} \times 10^{24}$	f (in Hz)	$h_0^{90\%} \times 10^{24}$
1249.717	5.1 ± 1.0	1250.217	5.0 ± 1.0	1250.717	5.1 ± 1.0	1251.217	5.1 ± 1.0
1251.717	5.0 ± 1.0	1252.217	5.2 ± 1.1	1252.717	5.0 ± 1.0	1253.217	5.0 ± 0.9
1253.717	5.0 ± 0.9	1254.217	5.0 ± 0.9	1254.717	5.2 ± 1.0	1255.217	5.0 ± 0.9
1255.717	5.0 ± 0.9	1256.217	5.0 ± 0.9	1256.717	5.0 ± 0.9	1257.217	5.0 ± 0.9
1257.717	5.0 ± 0.9	1258.217	5.2 ± 1.1	1258.717	5.1 ± 1.0	1260.717	5.1 ± 1.0
1261.217	5.1 ± 1.0	1261.717	5.0 ± 0.9	1262.217	5.2 ± 1.0	1262.717	5.0 ± 0.9
1263.217	5.0 ± 0.9	1263.717	5.1 ± 1.0	1264.217	5.0 ± 0.9	1264.717	5.0 ± 0.9
1265.217	5.0 ± 0.9	1265.717	5.0 ± 0.9	1266.217	5.0 ± 0.9	1266.717	5.0 ± 0.9
1267.217	5.1 ± 1.0	1267.717	5.2 ± 1.0	1268.217	5.2 ± 1.0	1268.717	5.0 ± 0.9
1269.217	5.1 ± 0.9	1269.717	5.1 ± 0.9	1270.217	5.1 ± 1.0	1270.717	5.1 ± 0.9
1271.217	5.1 ± 0.9	1271.717	5.1 ± 0.9	1272.217	5.2 ± 1.0	1272.717	5.1 ± 0.9
1273.217	5.2 ± 1.0	1273.717	5.1 ± 0.9	1274.217	5.1 ± 0.9	1274.717	5.1 ± 0.9
1275.217	5.1 ± 0.9	1275.717	5.4 ± 1.1	1276.217	5.1 ± 0.9	1276.717	5.2 ± 1.0
1277.217	5.2 ± 1.0	1277.717	5.1 ± 0.9	1278.217	5.1 ± 1.0	1278.717	5.1 ± 0.9
1279.217	5.1 ± 0.9	1279.717	5.0 ± 0.9	1280.217	5.2 ± 1.0	1280.717	5.0 ± 0.9
1281.217	5.0 ± 0.9	1281.717	5.2 ± 1.0	1282.217	5.3 ± 1.1	1282.717	5.1 ± 0.9
1283.217	5.1 ± 0.9	1283.717	5.1 ± 0.9	1284.217	5.3 ± 1.0	1284.717	5.1 ± 0.9
1285.217	5.1 ± 0.9	1285.717	5.2 ± 1.0	1286.217	5.4 ± 1.1	1286.717	5.2 ± 1.0
1287.217	5.1 ± 0.9	1287.717	5.1 ± 0.9	1288.217	5.1 ± 0.9	1288.717	5.1 ± 0.9

f (in Hz)	$h_0^{90\%} \times 10^{24}$	f (in Hz)	$h_0^{90\%} \times 10^{24}$	f (in Hz)	$h_0^{90\%} \times 10^{24}$	f (in Hz)	$h_0^{90\%} \times 10^{24}$
1289.217	5.2 ± 1.0	1289.717	5.4 ± 1.1	1290.217	5.1 ± 0.9	1290.717	5.1 ± 0.9
1291.217	5.1 ± 0.9	1291.717	5.4 ± 1.1	1292.217	5.1 ± 0.9	1292.717	5.1 ± 0.9
1293.217	5.1 ± 0.9	1293.717	5.3 ± 1.0	1294.217	5.2 ± 1.0	1294.717	5.1 ± 0.9
1295.217	5.2 ± 1.0	1295.717	5.1 ± 0.9	1296.217	5.2 ± 1.0	1296.717	5.3 ± 1.0
1297.217	5.1 ± 0.9	1297.717	5.3 ± 1.0	1298.217	5.4 ± 1.1	1298.717	5.2 ± 1.0
1299.217	5.1 ± 0.9	1299.717	5.4 ± 1.1	1300.217	5.2 ± 1.0	1300.717	5.1 ± 0.9
1301.217	5.3 ± 1.0	1301.717	5.2 ± 0.9	1302.217	5.2 ± 1.0	1302.717	5.2 ± 0.9
1303.217	5.2 ± 0.9	1303.717	5.3 ± 1.0	1304.217	5.3 ± 1.0	1304.717	5.2 ± 0.9
1305.217	5.2 ± 0.9	1305.717	5.2 ± 0.9	1306.217	5.2 ± 0.9	1306.717	5.3 ± 1.0
1307.217	5.3 ± 1.0	1307.717	5.5 ± 1.1	1308.217	5.2 ± 0.9	1308.717	5.4 ± 1.1
1309.217	5.2 ± 0.9	1309.717	5.3 ± 1.0	1310.217	5.5 ± 1.1	1310.717	5.4 ± 1.0
1311.217	5.2 ± 1.0	1311.717	5.3 ± 1.0	1312.217	5.2 ± 0.9	1312.717	5.3 ± 1.0
1313.217	5.4 ± 1.0	1313.717	5.2 ± 0.9	1314.217	5.2 ± 0.9	1314.717	5.4 ± 1.0
1315.217	5.5 ± 1.1	1315.717	5.5 ± 1.1	1316.217	5.2 ± 0.9	1316.717	5.2 ± 0.9
1317.217	5.4 ± 1.0	1317.717	5.5 ± 1.1	1318.217	5.2 ± 0.9	1318.717	5.3 ± 0.9
1320.717	5.3 ± 0.9	1321.217	5.3 ± 0.9	1321.717	5.2 ± 0.9	1322.217	5.4 ± 1.0
1322.717	5.2 ± 0.9	1323.217	5.2 ± 0.9	1323.717	5.3 ± 1.0	1324.217	5.4 ± 1.0
1324.717	5.2 ± 0.9	1325.217	5.5 ± 1.1	1325.717	5.4 ± 1.0	1326.217	5.2 ± 0.9
1326.717	5.5 ± 1.1	1327.217	5.2 ± 0.9	1327.717	5.2 ± 0.9	1328.217	5.2 ± 0.9
1328.717	5.4 ± 1.0	1329.217	5.2 ± 0.9	1329.717	5.4 ± 1.0	1330.217	5.2 ± 0.9
1330.717	5.4 ± 1.0	1331.217	5.3 ± 1.0	1331.717	5.2 ± 0.9	1332.217	5.2 ± 0.9
1332.717	5.2 ± 0.9	1333.217	5.2 ± 0.9	1333.717	5.2 ± 0.9	1334.217	5.4 ± 1.0
1334.717	5.2 ± 0.9	1335.217	5.2 ± 0.9	1335.717	5.4 ± 1.0	1336.217	5.3 ± 0.9
1336.717	5.3 ± 1.0	1337.217	5.3 ± 1.0	1337.717	5.3 ± 0.9	1338.217	5.6 ± 1.1
1338.717	5.3 ± 0.9	1339.217	5.3 ± 1.0	1339.717	5.4 ± 1.0	1340.217	5.3 ± 0.9
1340.717	5.4 ± 1.0	1341.217	5.3 ± 0.9	1341.717	5.3 ± 0.9	1342.217	5.3 ± 0.9
1342.717	5.4 ± 1.0	1343.217	5.6 ± 1.1	1343.717	5.3 ± 0.9	1344.217	5.3 ± 0.9
1344.717	5.4 ± 1.0	1345.217	5.4 ± 1.0	1345.717	5.3 ± 0.9	1346.217	5.3 ± 0.9
1346.717	5.3 ± 0.9	1347.217	5.3 ± 0.9	1347.717	5.6 ± 1.2	1348.217	5.3 ± 0.9
1348.717	5.3 ± 0.9	1349.217	5.4 ± 1.0	1349.717	5.4 ± 1.0	1350.217	5.3 ± 0.9
1350.717	5.3 ± 0.9	1351.217	5.4 ± 1.0	1351.717	5.4 ± 1.0	1352.217	5.3 ± 0.9
1352.717	5.3 ± 0.9	1353.217	5.3 ± 0.9	1353.717	5.3 ± 0.9	1354.217	5.3 ± 0.9
1354.717	5.6 ± 1.2	1355.217	5.4 ± 1.0	1355.717	5.3 ± 0.9	1356.217	5.3 ± 0.9
1356.717	5.5 ± 1.1	1357.217	5.6 ± 1.1	1357.717	5.3 ± 0.9	1358.217	5.3 ± 0.9
1358.717	5.3 ± 0.9	1359.217	5.3 ± 0.9	1359.717	5.5 ± 1.1	1360.217	5.3 ± 0.9
1360.717	5.4 ± 1.0	1361.217	5.5 ± 1.1	1361.717	5.3 ± 0.9	1362.217	5.3 ± 0.9
1362.717	5.7 ± 1.2	1363.217	5.4 ± 0.9	1363.717	5.4 ± 0.9	1364.217	5.4 ± 0.9
1364.717	5.5 ± 1.1	1365.217	5.4 ± 0.9	1365.717	5.4 ± 0.9	1366.217	5.4 ± 1.1
1366.717	5.4 ± 0.9	1367.217	5.4 ± 0.9	1367.717	5.5 ± 1.1	1368.217	5.5 ± 1.1
1368.717	5.5 ± 1.1	1369.217	5.7 ± 1.1	1369.717	5.4 ± 0.9	1370.217	5.5 ± 1.1
1370.717	5.4 ± 0.9	1371.217	5.4 ± 0.9	1371.717	5.5 ± 1.1	1372.217	5.4 ± 0.9
1372.717	5.9 ± 1.1	1373.217	5.7 ± 1.2	1373.717	5.5 ± 1.0	1374.217	6.1 ± 1.2
1374.717	5.7 ± 1.1	1375.217	5.5 ± 1.0	1375.717	5.5 ± 1.1	1376.217	5.4 ± 0.9
1376.717	5.7 ± 1.1	1377.217	5.5 ± 1.0	1377.717	5.6 ± 1.1	1378.217	5.7 ± 1.0
1378.717	5.5 ± 1.0	1380.717	5.5 ± 1.1	1381.217	5.4 ± 0.9	1381.717	5.7 ± 1.2
1382.217	5.4 ± 0.9	1382.717	5.5 ± 1.1	1383.217	5.4 ± 0.9	1383.717	5.5 ± 1.1
1384.217	5.4 ± 0.9	1384.717	5.4 ± 0.9	1385.217	5.5 ± 1.1	1385.717	5.4 ± 0.9
1386.217	5.6 ± 1.1	1386.717	5.7 ± 1.1	1387.217	5.6 ± 1.0	1387.717	5.5 ± 1.0
1388.717	5.7 ± 1.1	1389.217	5.8 ± 1.2	1389.717	5.5 ± 1.0	1390.217	5.6 ± 1.1
1390.717	5.9 ± 1.2	1391.217	6.1 ± 1.1	1391.717	5.6 ± 1.0	1392.217	5.8 ± 1.2
1392.717	5.6 ± 1.1	1393.217	5.8 ± 1.2	1393.717	5.5 ± 1.0	1394.217	5.6 ± 1.1
1394.717	5.5 ± 1.0	1395.217	5.5 ± 1.0	1395.717	5.5 ± 1.0	1396.217	5.5 ± 1.0
1396.717	5.5 ± 1.0	1397.217	5.6 ± 1.1	1397.717	5.6 ± 1.1	1398.217	5.6 ± 1.1

f (in Hz)	$h_0^{90\%} \times 10^{24}$	f (in Hz)	$h_0^{90\%} \times 10^{24}$	f (in Hz)	$h_0^{90\%} \times 10^{24}$	f (in Hz)	$h_0^{90\%} \times 10^{24}$
1398.717	5.5 ± 1.0	1399.217	5.5 ± 1.0	1399.717	5.8 ± 1.2	1400.717	5.8 ± 1.2
1401.217	5.8 ± 1.2	1401.717	5.8 ± 1.1	1402.217	5.5 ± 1.0	1402.717	5.5 ± 1.0
1403.217	5.5 ± 1.0	1403.717	5.5 ± 1.0	1404.217	5.5 ± 1.0	1404.717	5.8 ± 1.2
1405.217	5.7 ± 1.1	1405.717	5.5 ± 1.0	1406.217	5.5 ± 1.0	1406.717	5.6 ± 1.1
1407.217	5.5 ± 1.0	1407.717	5.7 ± 1.1	1408.217	5.5 ± 1.0	1408.717	5.6 ± 1.1
1409.217	5.5 ± 1.0	1409.717	5.5 ± 1.0	1410.217	5.5 ± 1.0	1410.717	5.5 ± 1.0
1411.217	5.5 ± 1.0	1411.717	5.6 ± 1.1	1412.217	5.5 ± 1.0	1412.717	5.6 ± 1.1
1413.217	5.5 ± 1.0	1413.717	5.5 ± 1.0	1414.217	5.5 ± 1.0	1414.717	5.6 ± 1.1
1415.217	5.5 ± 1.0	1415.717	5.6 ± 1.0	1416.217	5.7 ± 1.1	1416.717	5.6 ± 1.1
1417.217	5.7 ± 1.1	1417.717	5.6 ± 1.0	1418.217	5.6 ± 1.0	1418.717	5.7 ± 1.1
1419.217	5.6 ± 1.0	1419.717	5.6 ± 1.0	1420.217	5.6 ± 1.0	1420.717	5.6 ± 1.0
1421.217	5.8 ± 1.1	1421.717	5.6 ± 1.0	1422.217	5.6 ± 1.0	1422.717	5.6 ± 1.0
1423.217	5.6 ± 1.0	1423.717	5.6 ± 1.0	1424.217	5.7 ± 1.1	1424.717	5.6 ± 1.0
1425.217	5.6 ± 1.0	1425.717	5.6 ± 1.0	1426.217	5.7 ± 1.1	1426.717	5.8 ± 1.1
1427.217	5.8 ± 1.1	1427.717	5.6 ± 1.0	1428.217	5.8 ± 1.1	1428.717	5.8 ± 1.1
1429.217	5.8 ± 1.1	1429.717	5.8 ± 1.1	1430.217	5.6 ± 1.0	1430.717	5.6 ± 1.0
1431.217	5.6 ± 1.0	1431.717	5.6 ± 1.0	1432.217	5.6 ± 1.0	1432.717	5.6 ± 1.0
1433.217	5.6 ± 1.0	1433.717	6.0 ± 1.2	1434.217	5.8 ± 1.1	1434.717	5.8 ± 1.1
1435.217	5.6 ± 1.0	1435.717	5.6 ± 1.0	1436.217	5.8 ± 1.1	1436.717	5.8 ± 1.1
1437.217	5.6 ± 1.0	1437.717	5.8 ± 1.1	1438.217	5.9 ± 1.1	1438.717	5.8 ± 1.1
1440.717	5.7 ± 1.0	1441.217	5.7 ± 1.0	1441.717	5.7 ± 1.0	1442.217	5.7 ± 1.1
1442.717	5.9 ± 1.2	1443.217	5.7 ± 1.0	1443.717	5.7 ± 1.0	1444.217	5.7 ± 1.1
1444.717	5.7 ± 1.0	1445.217	5.7 ± 1.0	1445.717	5.7 ± 1.0	1446.217	5.7 ± 1.0
1446.717	5.8 ± 1.1	1447.217	5.7 ± 1.0	1447.717	5.7 ± 1.0	1448.217	5.7 ± 1.0
1448.717	5.9 ± 1.1	1449.217	5.8 ± 1.1	1449.717	5.7 ± 1.0	1450.217	5.7 ± 1.0
1450.717	5.8 ± 1.1	1451.217	5.7 ± 1.0	1451.717	6.0 ± 1.2	1452.217	5.7 ± 1.0
1452.717	5.7 ± 1.0	1453.217	5.9 ± 1.1	1453.717	5.8 ± 1.1	1454.217	5.8 ± 1.1
1454.717	5.7 ± 1.0	1455.217	5.8 ± 1.1	1455.717	5.7 ± 1.0	1456.217	6.0 ± 1.2
1456.717	5.9 ± 1.1	1457.217	5.7 ± 1.0	1457.717	5.7 ± 1.0	1458.217	6.0 ± 1.2
1458.717	5.7 ± 1.0	1459.217	5.8 ± 1.1	1459.717	5.7 ± 1.0	1460.217	5.8 ± 1.1
1460.717	5.7 ± 1.0	1461.217	5.7 ± 1.0	1461.717	5.7 ± 1.0	1462.217	5.7 ± 1.0
1462.717	5.7 ± 1.0	1463.217	5.7 ± 1.0	1463.717	5.7 ± 1.0	1464.217	5.7 ± 1.0
1464.717	5.7 ± 1.0	1465.217	5.8 ± 1.1	1465.717	5.9 ± 1.1	1466.217	5.7 ± 1.0
1466.717	5.8 ± 1.1	1467.217	5.7 ± 1.0	1467.717	5.8 ± 1.1	1468.217	5.8 ± 1.1
1468.717	5.9 ± 1.1	1469.217	5.8 ± 1.0	1469.717	5.8 ± 1.0	1470.217	6.0 ± 1.2
1470.717	5.8 ± 1.0	1471.217	5.8 ± 1.0	1471.717	5.8 ± 1.0	1472.217	5.8 ± 1.0
1472.717	5.8 ± 1.0	1473.217	6.1 ± 1.3	1473.717	5.9 ± 1.1	1474.217	5.9 ± 1.1
1474.717	6.1 ± 1.2	1475.217	5.8 ± 1.0	1475.717	6.1 ± 1.3	1476.217	6.0 ± 1.2
1476.717	5.8 ± 1.0	1477.217	5.8 ± 1.0	1477.717	6.1 ± 1.2	1478.217	5.9 ± 1.1
1478.717	5.8 ± 1.0	1479.217	5.9 ± 1.1	1479.717	6.0 ± 1.2	1480.217	5.8 ± 1.0
1480.717	5.9 ± 1.1	1481.217	5.8 ± 1.0	1481.717	5.8 ± 1.0	1482.217	5.8 ± 1.0
1482.717	5.8 ± 1.0	1483.217	5.8 ± 1.0	1483.717	5.8 ± 1.0	1484.217	5.9 ± 1.1
1484.717	5.8 ± 1.0	1485.217	6.1 ± 1.2	1485.717	6.0 ± 1.2	1486.217	5.8 ± 1.0
1486.717	5.9 ± 1.1	1487.217	5.8 ± 1.0	1487.717	5.9 ± 1.1	1488.217	5.8 ± 1.0
1488.717	5.8 ± 1.0	1489.217	6.1 ± 1.2	1489.717	5.8 ± 1.0	1490.217	5.9 ± 1.1
1490.717	5.8 ± 1.0	1491.217	5.8 ± 1.0	1491.717	5.8 ± 1.0	1492.217	5.8 ± 1.0
1492.717	5.8 ± 1.0	1493.217	5.8 ± 1.0	1493.717	5.9 ± 1.1	1494.217	5.8 ± 1.0
1494.717	5.9 ± 1.1	1495.217	5.8 ± 1.0	1495.717	6.1 ± 1.2	1496.217	5.9 ± 1.0
1496.717	5.9 ± 1.0	1497.217	5.9 ± 1.0	1497.717	6.0 ± 1.2	1498.217	6.0 ± 1.2
1498.717	6.2 ± 1.3	–	–	–	–	–	–

TABLE II. Left column denotes the starting frequency of each 0.5 Hz signal-frequency band in which we set upper-limits; right column states the upper-limit value i.e. $h_0^{90\%}$, for that 0.5 Hz band. Note: the $h_0^{90\%}$ values quoted here include additional 10% uncertainty introduced by data calibration procedure.

2. Detector Lines

Source	f (Hz)	Harmonics	LFS (Hz)	HFS (Hz)	IFO
Power Mains	60.0	5	1.0	1.0	L,H
Violin Mode	1373.75	1	0.1	0.1	H
Violin Mode	1374.44	1	0.1	0.1	H
Violin Mode	1377.14	1	0.1	0.1	H
Violin Mode	1378.75	1	0.1	0.1	H
Violin Mode	1379.52	1	0.1	0.1	H
Violin Mode	1389.06	1	0.06	0.06	H
Violin Mode	1389.82	1	0.07	0.07	H
Violin Mode	1391.5	1	0.2	0.2	H
Violin Mode	1372.925	1	0.075	0.075	L
Violin Mode	1374.7	1	0.1	0.1	L
Violin Mode	1375.2	1	0.1	0.1	L
Violin Mode	1378.39	1	0.1	0.1	L
Violin Mode	1387.4	1	0.05	0.05	L
Violin Mode	1388.5	1	0.3	0.3	L

TABLE III. Instrumental lines identified and cleaned before the Einstein@Home analysis. The different columns represent: (I) the source of the line; (II) the central frequency of the instrumental line; (III) the number of harmonics in the signal-frequency range, i.e. between 1249.7 Hz and 1499.7 Hz; (IV) Low-Frequency-Side (LFS) of the knockout band; (V) High-Frequency-Side (HFS) of the knockout band; (VI) the interferometer where the instrumental lines were identified. Note that when there are higher harmonics present, the knockout bandwidth remains constant.

3. Signal-frequency ranges and Data Quality

Source	Mixed (Isolated)	Mixed (Left)	All Fake Data	Mixed (Right)	IFO
Power Mains	– –	1258.7976 – 1259.2024	1259.2024 – 1260.7974	1260.7974 – 1261.2026	H,L
Power Mains	– –	1318.7915 – 1319.2085	1319.2085 – 1320.7913	1320.7913 – 1321.2087	H,L
Violin Mode	1372.6360 – 1373.2140	– –	– –	– –	L
Violin Mode	1373.4359 – 1374.0641	– –	– –	– –	H
Violin Mode	1374.1259 – 1375.5142	– –	– –	– –	H,L
Violin Mode	1376.8256 – 1377.4554	– –	– –	– –	H
Violin Mode	1378.0755 – 1379.0646	– –	– –	– –	H,L
Violin Mode	1379.2054 – 1379.8347	– –	– –	– –	H
Power Mains	– –	1378.7854 – 1379.2146	1379.2146 – 1380.7852	1380.7852 – 1381.2148	H,L
Violin Mode	1387.1346 – 1387.6655	– –	– –	– –	L
Violin Mode	– –	1387.9845 – 1388.4155	1388.4155 – 1388.5844	1388.5844 – 1389.0156	H,L
Violin Mode	1388.7844 – 1389.3356	– –	– –	– –	H,L
Violin Mode	1389.5343 – 1390.1057	– –	– –	– –	H
Violin Mode	1391.0842 – 1391.9159	– –	– –	– –	H,L
Power Mains	– –	1438.7793 – 1439.2207	1439.2207 – 1440.7791	1440.7791 – 1441.2209	H,L
Power Mains	– –	1498.7732 – 1499.2268	1499.2268 – 1499.7170	– –	H,L

TABLE IV. Signal-frequency ranges where the results might have contributions from fake data. When the results are entirely due to artificial data, the band is listed in the "All Fake Data" column; bands where the results comprise of contributions from both fake and real data are listed in the other three columns. The "Mixed (Left)" and "Mixed (Right)" columns are populated only when there is a matching "All Fake Data" entry, which highlights the same physical cause for the fake data, i.e. the cleaning. The "Mixed (Isolated)" column lists isolated ranges of mixed data. The list of input data frequencies where the data was substituted with artificial noise are given in Table III.

4. Omitted 50 mHz bands from Signal-frequency

f_{start} (in Hz)	f_{end} (in Hz)	Type	f_{start} (in Hz)	f_{end} (in Hz)	Type
1258.617	1258.717	D	1259.217	1260.717	C
1291.017	1291.067	D	1292.567	1292.867	D
1293.267	1293.567	D	1293.917	1294.217	D
1296.367	1296.817	D	1297.517	1297.717	D
1298.667	1298.967	D	1313.467	1313.517	D
1318.567	1318.667	D	1319.217	1320.717	C
1372.867	1373.167	D	1376.417	1376.817	D
1378.517	1378.617	D	1379.217	1380.717	C
1382.567	–	D	1387.317	–	D
1387.767	1388.217	D	1388.417	1388.517	C
1389.467	–	D	1389.767	1390.217	D
1390.467	1390.867	D	1390.967	1391.117	D
1395.217	1395.467	D	1398.417	1398.667	D
1399.967	1400.867	D	1400.967	1401.267	D
1438.417	1438.517	D	1439.267	1440.717	C
1453.467	1453.517	D	1454.967	1455.067	D
1498.317	1498.467	D	1499.267	1499.667	C

TABLE V. 50 mHz search-frequency bands that were identified as "disturbed" based on Visual Inspection (Type D), or where the results were produced from "All Fake Data", as detailed in Table IV (Type C). Both sets of bands (Type D and C) were excluded from the analysis. The first two columns list the starting frequency of the first and last 50 mHz band in the contiguous range of excluded bands.

[1] J Aasi *et al* (LIGO Scientific Collaboration). *Directed search for continuous gravitational waves from the Galactic center*. **Phys. Rev. D**, 88(10):102002, 2013.

[2] J Aasi *et al* (LIGO Scientific Collaboration). *Einstein@Home all-sky search for periodic gravitational waves in LIGO S5 data*. **Phys. Rev. D**, 87(8):042001, 2013.

[3] J Abadie *et al* (LIGO Scientific Collaboration). *Calibration of the LIGO gravitational wave detectors in the fifth science run*. **Nucl. Instrum. Meth. A**, 624(1):223–240, 2010.

[4] B Abbot *et al* (LIGO Scientific Collaboration). *Searches for periodic gravitational waves from unknown isolated sources and Scorpius X-1: Results from the second LIGO science run*. **Phys. Rev. D**, 76(8):082001, 2007.

[5] B Abbot *et al* (LIGO Scientific Collaboration). *All-sky search for periodic gravitational waves in LIGO S4 data*. **Phys. Rev. D**, 77(2):022001, 2008.

[6] B Abbot *et al* (LIGO Scientific Collaboration). *LIGO: the Laser Interferometer Gravitational-Wave Observatory*. **Rep. Prog. Phys.**, 72(7):076901, 2009.

[7] B Abbot *et al* (LIGO Scientific Collaboration). *All-Sky LIGO Search for Periodic Gravitational Waves in the Early Fifth-Science-Run Data*. **Phys. Rev. Lett.**, 102 (11):111102, 2009.

[8] B Abbot *et al* (LIGO Scientific Collaboration). *All-sky search for periodic gravitational waves in the full S5 LIGO data*. **Phys. Rev. D**, 85(2):022001, 2012.

[9] B Abbot *et al* (LIGO Scientific Collaboration). *Results of the deepest all-sky survey for continuous gravitational waves on LIGO S6 data running on the Einstein@Home volunteer distributed computing project*. **arXiv:1606.09619**, 2016.

[10] B Abbot *et al* (LIGO Scientific Collaboration). *Comprehensive All-sky Search for Periodic Gravitational Waves in the Sixth Science Run LIGO Data*. **arXiv:1605.03233**, 2016.

[11] C Cutler and B F Schutz. *Generalized $\mathcal{F}$-statistic: Multiple detectors and multiple gravitational wave pulsars*. **Phys. Rev. D**, 72(6):063006, 2005.

[12] N K Johnson-McDaniel and B J Owen. *Maximum elastic deformations of relativistic stars*. **Phys. Rev. D**, 84(4): 044004, 2013.

[13] D Keitel. *Robust semicoherent searches for continuous gravitational waves with noise and signal models including hours to days long transients*. **Phys. Rev. D**, 93(8): 084024, 2016.

[14] J Ming *et al*. *Optimal directed searches for continuous gravitational waves*. **Phys. Rev. D**, 93(6):064011, 2016.

[15] H J Pletsch. *Parameter-space correlations of the optimal statistic for continuous gravitational-wave detection*. **Phys. Rev. D**, 78(10):102005, 2008.

[16] H J Pletsch. *Parameter-space metric of semicoherent searches for continuous gravitational waves*. **Phys. Rev. D**, 82(4):042002, 2010.

[17] R Prix, S Giampanis, and C Messenger. *Search method for long-duration gravitational-wave transients from neutron stars*. **Phys. Rev. D**, 84(2):023007, 2011.

[18] A Singh. *Gravitational Wave transient signal emission via Ekman Pumping in Neutron Stars during post-glitch relaxation phase*. **arXiv:1605.08420**, 2016.

[19] K Wette. *Estimating the sensitivity of wide-parameter-space searches for gravitational-wave pulsars*. **Phys. Rev. D**, 85(4):042003, 2012.

[20] S Zhu *et al.* *An Einstein@home search for continuous gravitational waves from Cassiopeia A*. **arXiv:1608.07589**, 2016.